Master's Thesis

Efficient Third Harmonic Generation from Polaritonic Metasurfaces with Monopole-Dipole Interaction

Choi. Dongrye

Department of Electrical Engineering

Graduate School of UNIST

2021

Efficient Third Harmonic Generation from Polaritonic Metasurfaces with Monopole-Dipole Interaction

Choi. Dongrye

Department of Electrical Engineering

Graduate School of UNIST

Efficient Third Harmonic Generation from Polaritonic Metasurfaces with Monopole-Dipole Interaction

A thesis/dissertation
submitted to the Graduate School of UNIST
in partial fulfillment of the
requirements for the degree of
Master of Science

Choi. Dongrye

2020.12.18 of submission
Approved by

_____

Advisor
Jongwon Lee

Efficient Third Harmonic Generation from Polaritonic Metasurfaces with Monopole-Dipole Interaction

Choi. Dongrye

This certifies that the thesis/dissertation of Choi. Dongrye

is approved.

2020.12. 18 of submission

signature

_____

Advisor: Jongwon Lee

signature

_____

typed name: Joo-Yun Jung

signature

_____

typed name: Jiwon Chang

Abstract

The advance of Metasurfaces provides new possibilities to develop various optical applications with promising alternatives of traditional optical devices. The ultrathin and ultracompact feature gives us a new possibility to develop novel optical devices overcoming the conventional limitation. In this novel functionality open a new dimension for research of nonlinear optical applications.

In nonlinear optics, nonlinear metasurface provide a new degree-of-freedom in generating and manipulating nonlinear optical responses at deeply subwavelength scale. Subwavelength-thin nonlinear metasurfaces have been developed for demonstrating various nonlinear properties, such as the relaxed phase matching condition which is difficult to obtain with conventional nonlinear crystals, frequency conversion with high efficiency, and local control of nonlinear response. Although there have been various studies on nonlinear metasurfaces, higher frequency conversion efficiency is still required to be used as a practical level of optical devices.

In this thesis, I proposed and experimentally demonstrated nonlinear polaritonic metasurface based on monopole-like modes induced in a nanoantenna structure for highly efficient Third Harmonic Generation response. Using an epitaxial grown Multi-Quantum-Well layer as a nonlinear medium, giant 3^{rd} order nonlinear susceptibility which is 4-5 orders of magnitude higher than traditional nonlinear materials was obtained and the giant nonlinear response was used in coupling with the plasmonic nanoresonators to build the nonlinear polaritonic metasurface. The proposed nonlinear polaritonic metasurface can be applied to increase the third harmonic generation efficiency and other nonlinear frequency conversion processes such as sum frequency generation, difference frequency generation and second harmonic generation.

Contents

LIST OF FIGURES

LIST OF Tables

I. Introduction

1.1 Nonlinearity

1.1.1 Nonlinear polarizations

In the linear optics case, the induced polarization depends on the electric field strength that can often be defined as[8]

$$P(t) = \varepsilon_0 \chi^{(1)} E(t) \tag{1.1.1}$$

The constant $\chi^{(1)}$,ε_0 indicate as linear susceptibility and permittivity of free space respectably. However, in nonlinear optics, the polarization dependence described on a power series with electric field strength $E(t)$ when incident electric fields are strong enough to drive beyond the regime of a linear.

$$\begin{aligned} P(t) &= \varepsilon_0 \left[\chi^{(1)} E(t) + \chi^{(2)} E^2(t) + \chi^{(3)} E^3(t) + \cdots \right] \\ &\equiv P^{(1)}(t) + P^{(2)}(t) + P^{(3)}(t) + \cdots . \end{aligned} \tag{1.1.2}$$

$\chi^{(2)}$ and $\chi^{(3)}$ are known as second and third order nonlinear susceptibility tensor element. In a conventional case, the first linear term is only important and the other components have only response when the E field's harmonic frequencies match with the polarization oscillation. However, with increasing field intensity, the nonlinear susceptibility, $\chi^{(2)}$ and $\chi^{(3)}$ can become sufficiently large, then the material response becomes nonlinear.[9]

1.1.2 Third Harmonic Generation

Third harmonic generation (THG) is one of the famous nonlinear optical phenomena. The three photons with the same frequency interact with the nonlinear material including natural materials like molecules, nonlinear crystal, and plasmonic materials that is the new arisen research area. In this interaction of photons in nonlinear medium, incident light converted to the energies at tripled frequency, generating generation of third harmonic light. This frequency conversion property as it can said to be nonlinear optical effect make an important implementation of noble photonic functionalities.

(a) (b)

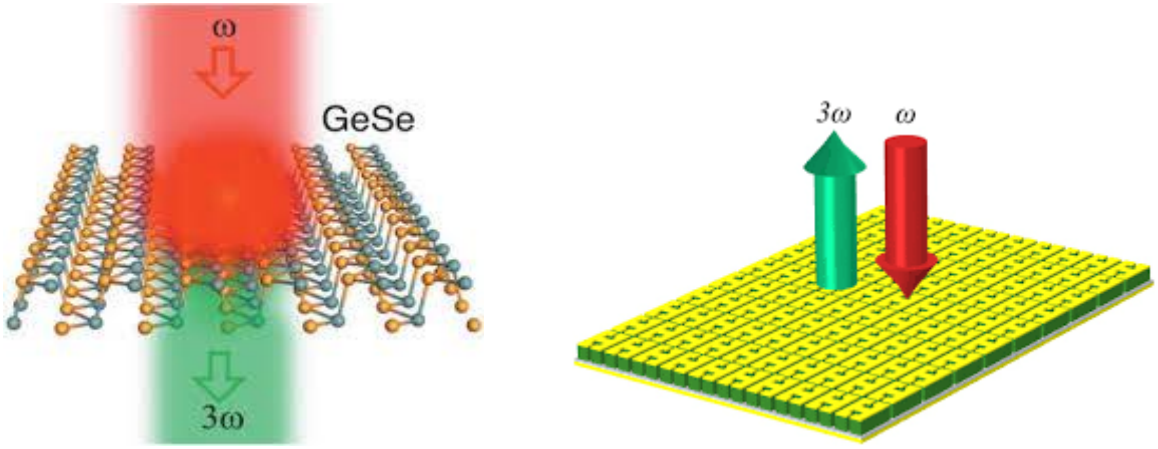

Figure 1.1.1 (a)THG from the nonlinear crystal [24] (b)THG from nonlinear metasurface [4]

Third Harmonic Generation realized as various applications in photonics. For example, chemistry, material science, biosensing[2], nonlinear holography[1] and tunable optical transistor[23].However implementation of these potential applications is quite elusive. Since the nonlinear response in nature nonlinear materials are not strong enough to develop in applications so it needs necessarily strong bulk material to stand with the high intensity for experimentally checking the nonlinear signal, but in the large scale of bulk material, the reason for fundamental and harmonic signals has different propagation speeds inside the media. So, the generated harmonic signals at different points interfere destructively with each other. Therefore, phase matching techniques to compensate for optical dispersion[3] is necessary for this research with complicated phase matching step or separate research for it.

1.2Plasmonic Resonances

(a) (b)

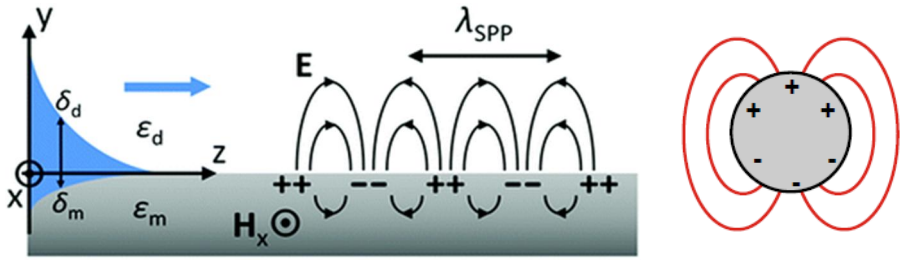

Figure1.2.1. Schematic of the plasmonic excitation (a)surface plasmon polaritons exists in meta-dielectric interface with electromagnetic fields. (b)localized surface plasmon

Optical property of metal is highly affected by the conduction band electron. This electron can interact with the electromagnetic wave. With forming an oscillation system, plasmon is excitation oscillation collectively. Surface Plasmon Polaritons (SPPs), in shortly, the phenomena of light and matter interaction in dielectric-metal interface. Generally, SPPs are surface wave that exists on a metal-dielectric interface. In the optical regime, the electromagnetic field of incident waves interacts with the plasma electron near the surface of the metal and therefore excites collective oscillation propagating along the interface. From boundary condition in dielectric-metal interface, dispersion relation can be derived. With only TM (Transverse Magnetic) mode can be induced excitation in metal layer, so the dispersion relation of SPP described as

$$k_{spp} = \frac{\omega}{c}\sqrt{\frac{\varepsilon_m \varepsilon_d}{\varepsilon_m + \varepsilon_d}} \qquad (1.2.1)$$

ε_m and ε_d are permittivities of dielectric and metal, k_0 is the light wavenumber and $k_{SPP} = k_x$, c indicates the speed of light and ω indicates angular frequency. For the SPP existing, $\frac{\varepsilon_m \varepsilon_d}{\varepsilon_m + \varepsilon_d}$ should be positive value, as the almost noble metals satisfy in spectral region of permittivity, the real part of ε_m should be negative. the dispersion relation of SPP implies $k_{spp} > k_0 = \frac{\omega}{c}$. It means SPs have larger k value than photon at same energy. Therefore, SPs cannot propagate free space.

When SPs takes place within the nanostructure, it is known as localized surface plasmon resonance (LSPR)[17]. In this case electron oscillation with resonance can be excited in propagating free space.

The collective behavior of local plasmons in nanoarrays has a coherent optical response, and the response is not limited to only one nanoparticle each. This homogenization leads to variation of effective

parameter as permittivity or permeability with strong and narrow spectral features. The optical spectrum of a nano-array depends on size, shape, and periodicity of the structures, which provides good flexibility and tunability of optical properties. It means by using plasmonic nanoarray, the optical properties can be engineered.

1.3 Metasurface

To transcend property compared with nature material, Metamaterials give an alternative to optical materials. With artificially designed meta-atoms, amplitude, phase, and polarization of scattered light from the structure can be engineered in a scale much shorter than the working wavelength as it can said to be like subwavelength scale. By properly designing the metaatoms into metamaterials, the goal for metamaterial can be achieved. For example, the negative refractive index, optical cloaking, meta lens. [Figure 1.3.1(a)-(c)]

Though metamateirals have drawn large amount of interesting research, their properties mostly rely on bulk response from spatially arranged meta-atoms. Therefore, in nonlinear research, it still has problem in phase matching issue. The difficulty does not be limited at this, there is more serious problems, like difficulty to fabricated and integrated with the applications.

(a) (b) (c)

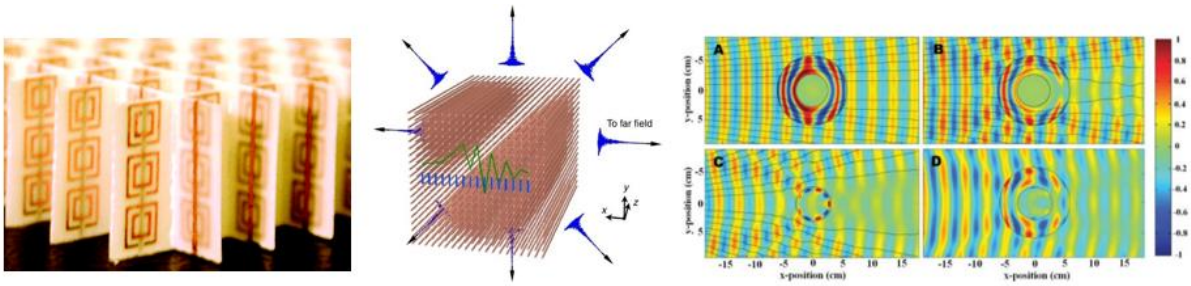

Figure1.3.1. metamaterial applications. (a) negative refractive index metamaterial.[10] (b) hyper metalens.[11] (c)optical clocking metamaterial [12]

Metasurfaces open new horizons in overcoming the limitation in scale with controlling the propagation of electromagnetic waves with the light-matter interactions down to subwavelength regime. Unlike metamaterials, metasurfaces can be defined as an optically thin layer of metamaterial, whose thickness is less than the operating wavelength, as it is specified as a 2D regime. The consisting of metasurface itself is same as metamaterial with each of meta-atom as an optical antenna. The metasurface consisting antennas(resonators) have flexibility in shape, composite materials, and periodicity, resulting in enough freedom in control the local field distribution and scattering of incident wave. Similar to metamaterials, novel features, such as reconfigurable light pathways[26], beamforming and on-chip optical radiation[25], can be achieved by integrating dynamically tunable components, gain medium, or nonlinear materials.

1.4 Giant Nonlinearity in MQWs based Nonlinear metasurface

When using MQWs in the nonlinear medium, The Third Harmonic peak intensity I_{3w} can be defined as[5]

$$I_{3w} = \frac{9}{16}\omega^2\eta_0^4\left(\varepsilon_0\chi_{ijkl}^{(3)eff}\right)^2 I_\omega^3 L^2 \tag{1.4.1}$$

ω indicates the input frequency, η_0 is $1/\varepsilon_0 c$, ε_0 is the permittivity in a vacuum, c indicates the speed of light in a vacuum, I_ω indicates intensity of the input beam, L indicates the nonlinear medium layer thickness, and $\chi_{ijkl}^{(3)eff}$ is susceptibility tensor element of nonlinear medium. When the dimensionality got lower in metasurfaces, easy to use thin film nonlinear research in which its thickness is subwavelength regime, the complex bulk phase matching condition almost removed and just need to phase matching only in parallel. This condition matched proper lens used. The problem is from the Equation (1.4.1) the nonlinear medium thickness is smaller than the wavelength, I_{3w} is proportional to the square with the thickness L, the subwavelength order thickness makes third-harmonic intensity got lowered. solve this problem, must need to make $\chi_{ijkl}^{(3)eff}$ get orders of larger value.

By designing the MQWs in proper way, it can be designed in Intersubband transition occurring with 3 or 4 energy bands. electron transits in quantized energy band in conduction band or valence band structure, it called Intersubband transition. The valence band case, the hole energy state separated in heavy hole and light hole, so it is difficult to be confined the high energy in valence band case. So almost intersubband transition research is designed in electron transition in conduction band with n-doping. The benefit of intersubband transition is got high density of state with narrow single peak with strong absorption. However, in MQW structure, electrons are quantized in only grown z-direction, the vertical direction of the surface. Therefore, the incident photon should be polarized in z-direction. For Third Harmonic Generation in MQWs, nonlinear susceptibility could be described as[5]

$$\chi_{zzzz}^{(3)}(\omega \to 3\omega) = N_e \frac{e^4}{\varepsilon_0{}^3} \frac{z_{12}z_{23}z_{34}z_{41}}{(\omega-\omega_{12}-i\gamma_{12})(2\omega-\omega_{13}-i\gamma_{13})(3\omega-\omega_{14}-i\gamma_{14})} \tag{1.4.2}$$

where, N_e is the average bulk doping density, ω is the input frequency, e is the electron charge, $\hbar\Upsilon_{ij}$ is transition linewidth, $\hbar\omega_{ij}$ is transition energy, and z_{ij} is dipole moment between energy states i and j. MQWs cannot be resonated in propagating free space electromagnetic field, so combined with the plasmonic structure to induced E_z field.

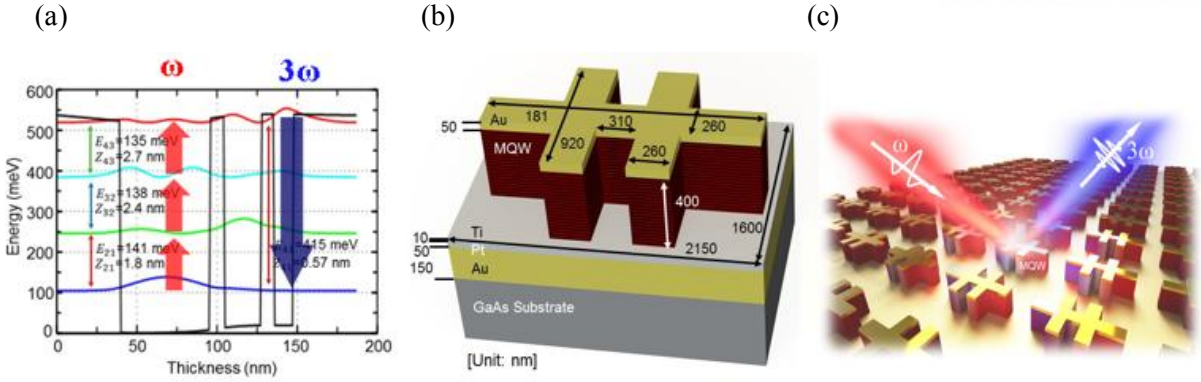

Figure1.4.1 Research of MQW based Nonlinear photonic metasurce for THG [6]

(a)Designed coupled three-quantum-well structure in period of conduction band diagram for giant 3rd order nonlinear responses. (b) Schematic of meta-atom designs. Unit cell structure of the plasmonic antenna. (c) Schematic of operation in metasurfce.

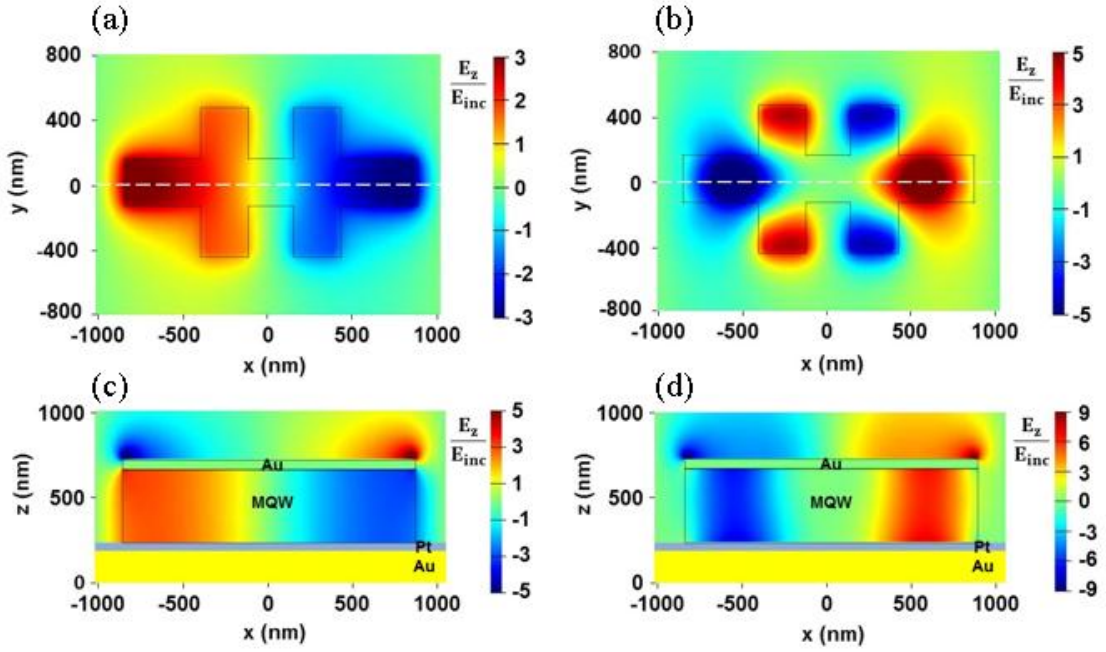

Figure1.4.2 FDTD mode profile results of the plasmonic nonlinear metasurfaces. (a)-(b) Top-view cross section of the normalized Ez field distribution on the resonator monitored in the MQW at the FF (ω) (a) and TH (3ω) (b) frequencies. (c)-(d) Side-view the normalized Ez field shown at the FF (c) and TH (d) frequencies.[6]

Using these MQWs based nonlinear photonic metasurfaces, the prior research has been done in our group.[6] This structure has unprecedented strong THG intensity and TH nonlinearity.

The effective $\chi^{(3)eff}$ of in the polarization of incident electromagnetic field of metasurface is defined with the $\chi^{(3)eff}$ of MQW itself and integrated value of induced z field as it called overlap factor,[6]

$$\chi_{ijkl}^{(3)eff} = \chi_{zzzz}^{(3)} \left\langle \frac{E_{z(i)}^{3\omega}}{E_{i(inc)}^{3\omega}} \cdot \frac{E_{z(j)}^{\omega}}{E_{j(inc)}^{\omega}} \cdot \frac{E_{z(k)}^{\omega}}{E_{k(inc)}^{\omega}} \cdot \frac{E_{z(l)}^{\omega}}{E_{l(inc)}^{\omega}} \right\rangle, (i,j,k,l = x,y) \qquad (1.4.3)$$

$\chi_{zzzz}^{(3)}$ is determined value by grown MQWs, but the overlap factor part can be increasing with the structure design optimizing. increasing this factor is quite important because third harmonic intensity is proportional squared to the $\chi^{(3)eff}$, the doubled overlap factor make the intensity four times higher. In this prior research, overlap factor reaches 1.4. However it has giant nonlinear response in THG, There are still areas to be improved. In this structure, strong interaction is only induced in the small area near the antenna edge. This makes a lot metal loss and quick saturation.

1.5 Motivation

Previous work has obtained the highest THG response using the MQW-based plasmonic structure, but a new resonator design to relax saturation is needed to improve the nonlinear response, i.e. to make a large overlap coefficient for high field enhancement. The traditional structure reaches fast to the saturation effect and metal loss get higher. For these two problems solved, the motivation for develop the prior research can be found in the Reference [18].

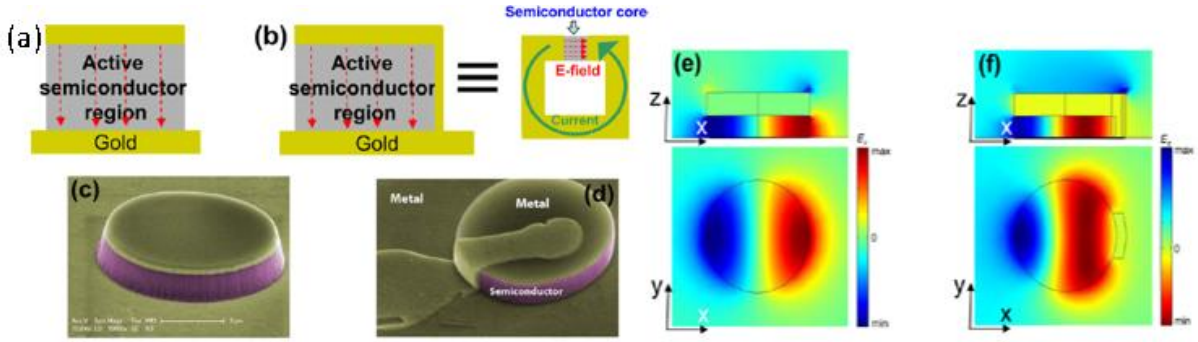

Figure1.5.1 (a) Scheme of a standard patch-cavity resonator (b) resonator able to operate on the monopolar resonance (c) Scanning electron microscope (SEM) image of a typical round patch cavity.

(d) SEM image of ability to make monopole mode resonator. (e) and (f) Side/top view of the field distribution of the resonators [18]

This research is making monopole-like mode for Terahertz generation by top-bottom gold. This top-bottom connected structure made newly mode, monopole-like mode. This mode has large region for E field enhancement, It is not the usual mode but by artificially connecting top-bottom metal which can make the electron move not in conventional way with make newly mode. Therefore in the side view, it is much like SRR (Split-ring resonator) magnetic dipole moment because of the electron moves top meal to bottom metal. However, in the top view, they give a chance to analyze as the potential for new mode interaction. This ‘monopole like’ mode makes large region for interaction. this combined with our prior research, I designed the structure of nonlinear photonic metasurface.

II. THG Metasurface with Monopole-Dipole Interaction

2.1 Simulation method Nonlinear Metasurfaces

2.1.1 Design of MQWs

The most important thing in MQW design for MBE growth is select materials that consist the MQW with lattice constant matching between barrier and well material. I have used AlInAs/InGaAs in my MQW structures: AlInAs bandgap energy is higher than InGaAs which means that AlInAs and InGaAs are barrier and well layer, respectively [Fig.3.1.1]. the effective mass in the barrier material AlInAs is significantly small, it is easier to confine equally spaced bound states not to make barrier problematically thin, and relatively small effective mass of GaInAs make advantage of large dipole matrix element compared with AlGaAs/GaAs for the same intersubband transition.[5]

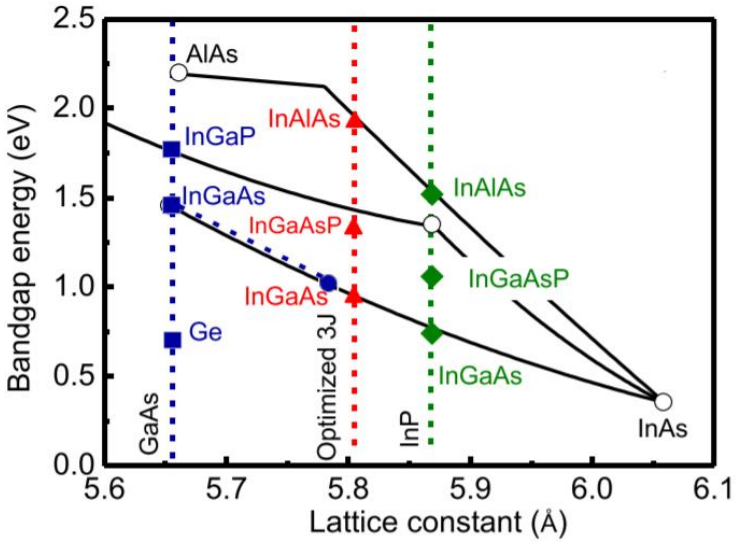

Figure.2.1.1 Energy band gap diagram as a function of lattice spacing for selected III-V compound semiconductor materials. The substrates' lattice spacings are represented by open circles.[5]

Layer	Material	[nm]	Ratio	Doping (cm^{-3})
1	InGaAs	300	$In_{0.53}Ga_{0.47}As$	
2	InP	100		
3	InGaAs	5	$In_{0.53}Ga_{0.47}As$	1.00×10^{18}
4	AlInAs	4	$Al_{0.48}In_{0.52}As$	

Start of 20 repeat periods				
5	AlInAs	4	$Al_{0.48}In_{0.52}As$	
6	InGaAs	4.6	$In_{0.53}Ga_{0.47}As$	4×10^{18}
7	AlInAs	1.2	$Al_{0.48}In_{0.52}As$	
8	InGaAs	2	$In_{0.53}Ga_{0.47}As$	
9	AlInAs	1.2	$Al_{0.48}In_{0.52}As$	
10	InGaAs	1.8	$In_{0.53}Ga_{0.47}As$	
11	AlInAs	4	$Al_{0.48}In_{0.52}As$	
End of repeat periods				
12	AlInAs	4	$Al_{0.48}In_{0.52}As$	
13	InGaAs	5	$In_{0.53}Ga_{0.47}As$	1.00×10^{18}

Table.2.1.1 MQW Growth sheet for Molecular Beam Epitaxy. The semi-insulating (100) InP substrate was used.

In order to have giant 2nd and 3rd order nonlinear susceptibilities, MQWs are used as a nonlinear medium.for design the multi quantum well structures for nonlinear intersubband transition, I used a program of Poisson-Schrodinger solver.[6] The layer 1-4 are spacer layer which protect the 5-11 MQW region. For 400nm of MQWs, these layers are repeated at 20 times. Before and after layer (4,12) of AlInAs are for considering repeating MQWs barrier width. The n-doping information is in three parts of layer, (3,6,13). The doping of 3,13 layer is for making good adhesion with metal as it means by doping on the non-metal region, the metallic property is given. The main doping layer is 6, the doped ground level electrons as I can say that in first well for nonlinear effect itself. Notice that the excessive doping on main doping layer 6, the first energy level could be disappeared.

(a) (b)

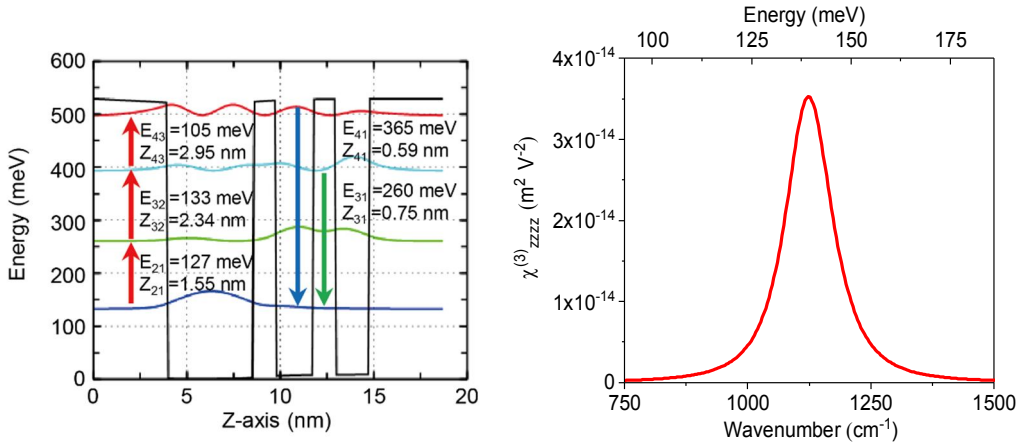

Figure2.1.2 (a)Designed coupled three-quantum-well structure in period of conduction band diagram for giant 3rd order nonlinear responses. Z_{ij} is the transition dipole moment element and E_{ij} is transition energy of the intersubband transitions between electron subbands i and j, respectively (b) As a function of the pump wavenumber, Third-order nonlinear susceptibility of the MQW structure in (a).

By design the structure to using the MQWs to use its property in high susceptibility with plasmonic cavity structure, it can be used with giant 3rd order nonlinear responses generate coherent THG in the far-field. From the Figure 2.2.2 (b) the $\chi^{(3)}_{zzzz}$ values can be checked as expected that were calculated by numerical calculation using the physical parameters extracted from the intersubband absorption measurement. $\chi^{(3)}_{zzzz}$ has maximum values of 2.27×10^{-14} m^2 V^{-2} near the 9 μm wavelength.

2.1.2Metasurface design

I used numerical code and commercial Finite-Difference Time-Domain solver (Matlab and Lumerical FDTD Solutions (ver. 8.19), respectively) for numerical simulations. The boundary condition setting is used perfectly matched layer (PML) boundary condition in the z-direction and periodic boundary condition in the x- and y-direction. The using gold layers were modeled as Drude metal with collision frequency of $\Gamma = 1.224 \times 10^{14}\mathrm{rad/s}$ and plasma frequency of $\omega_p = 1.378 \times 10^{16}\mathrm{rad/s}\Gamma = 1.224 \times 10^{14}\mathrm{rad/s}$. In MQW layer, by using calculated from the absorption measurement and parameter calculations set MQW constant for the in-plane and out-of-plane dielectric constants. To make monopole interaction meta-atom array for nonlinear photonic metasurfaces, three points should be confirmed. Firstly, this structure can confine high electric field on its structure with high E field enhancement. Secondly, considering the MQWs grown feature which makes it only have high susceptibility in normal to the surface, the structure can be induced high E_z field inside of the MQW regions (nonlinear media). At last, to make monopole mode the top-bottom metal should be connected with which it does not interact any other interaction except making the monopole mode.

(a) (b)

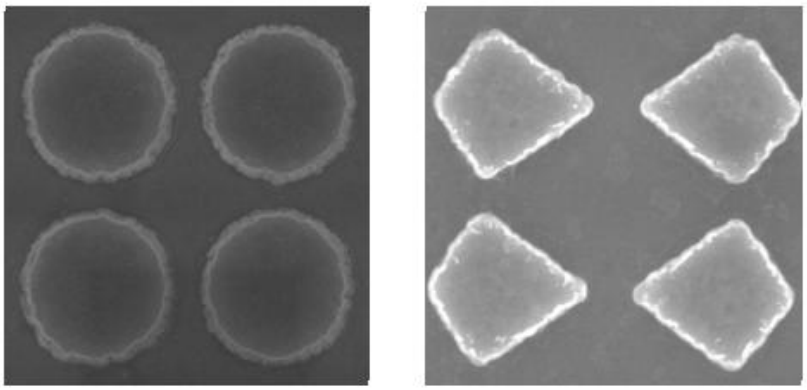

Figure2.1.3. Top-view of SEM image of metasurface resonators. (a)circular-shaped resonator (b)kite-shaped resonators.

I designed the resonator as the proper design to enhance large E-field. Start with the same design of Reference [18] in circular-shape, this shape can interact in large area, but it cannot be enhanced because high E field in edge, usually got quite high enhancement, is curve. Therefore, it is necessary to design the resonator that stand with the E field enhanced region wide and make enhancement got high. Considering the mentioned factors, for high E field enhancement occurring in incident electromagnetic

wave, change the design of resonator shape circle to rhombus shape. And with optimize this shape, kite shape selected.

Next step to design is confirmed the 'monopole mode' got formed when the top-bottom metal connected.

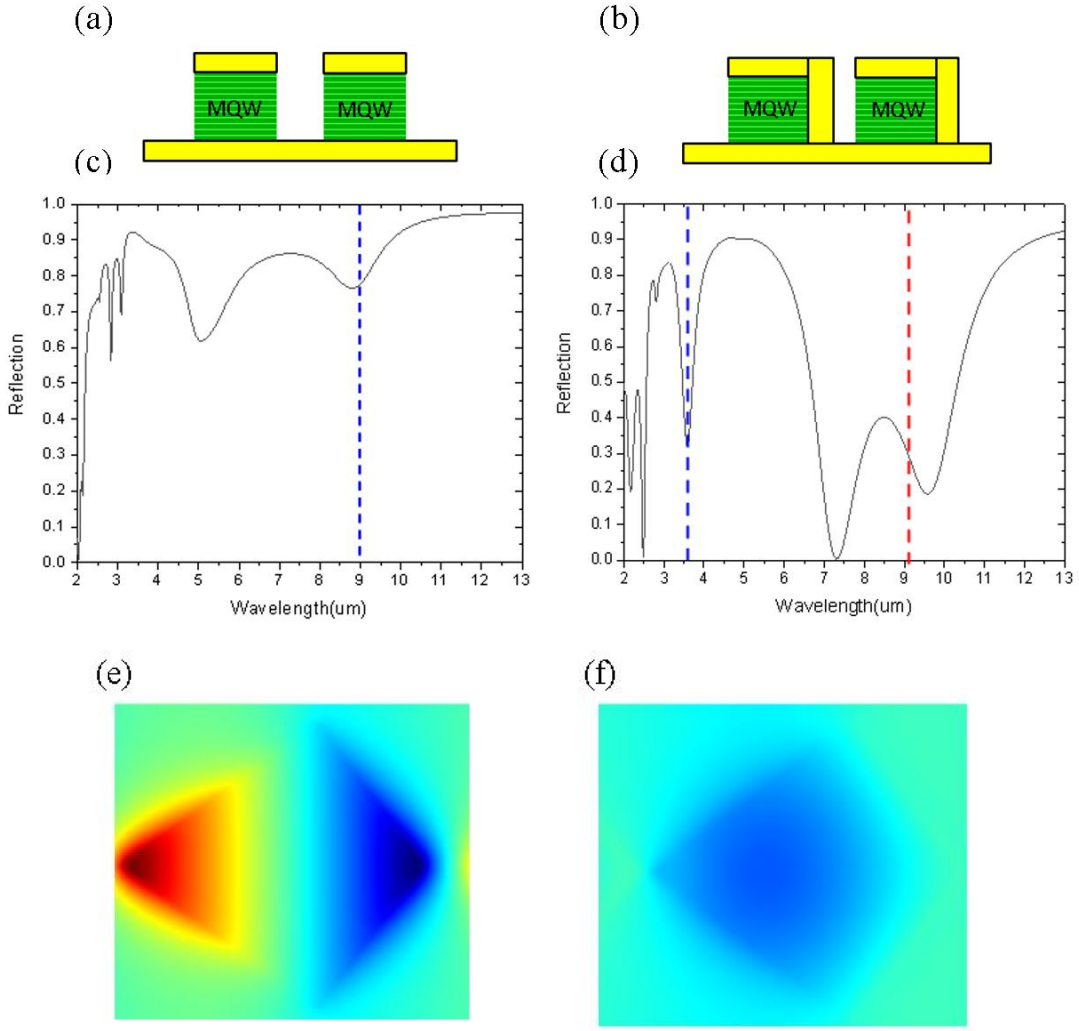

Figure2.1.4. (a)-(b) side-view schematic of of metasurface resonators. (a) standard plasmonic cavity antennas. (b)top-bottom metal connected plasmonic antennas (c)-(d) Finite Difference Time Domain (FDTD) simulation results of reflection. Red line means monopole mode profile can be shown, bule line means dipole mode shown. (c) case of non-connected top-bottom metal resonator's metasurface simulation result of reflection (d) case of top-bottom metal connected resonator's metasurface simulation result. (e) case of non-connected top-bottom metal resonator's metasurface simulation result of mode profile in 9um (f) case of top-bottom metal connected resonator's metasurface simulation result of mode profile in 9um

The difference between top-metal connected or not quite definite. Designed MQW absorption is 9um, it means the fundamental frequency is at 9um. Therefore, check the mode profile of 9um, Figure3.1.4. (e)and(f), besides the non-connected structure mode profile at 9um shown exact dipole mode file, it is clear that when connected top-bottom metal make monopole-like mode. But the interaction with that structure quite weak, and it is hard to optimize at 3um, the THG peak wavelength, in change of resonator dimension. So in this time, I considered the interaction between the resonators. It's quite simple change but the result quite unexpectable way. the pair of two resonators in mirror symmetric for interacting each other, The traditional dipole mode split in tow dipole modes.

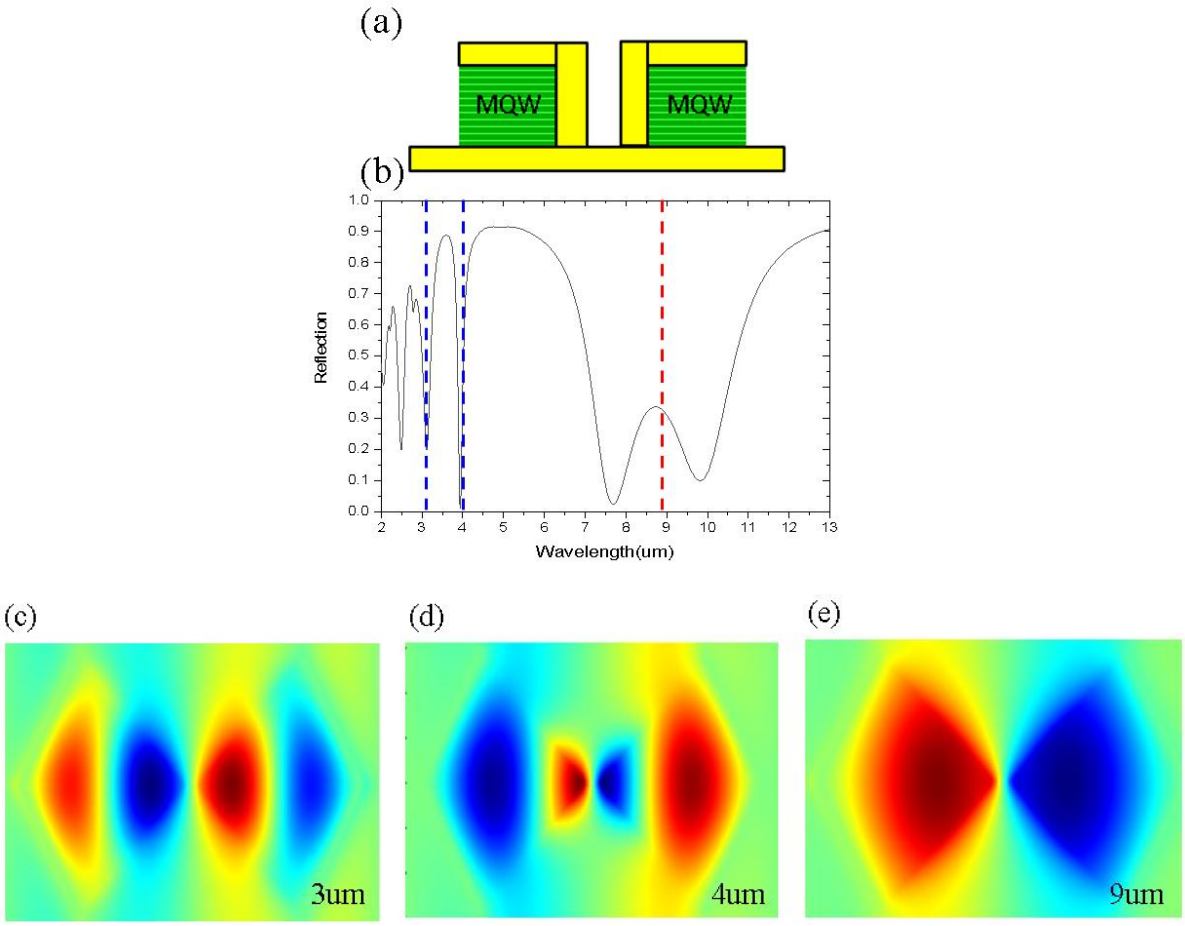

Figure2.1.5. (a) side-view schematic of of metasurface resonators. In this case, top-bottom metal connected pair of plasmonic antennas in mirror symmetric. (b) FDTD simulation results of reflection. Red line means monopole mode profile can be shown, bule line means dipole mode shown. (c)-(e) mode profile of monopole and dipole peak in pair.

the grounds of the resonator pair got interacted each other also can be checked by the mode profile in Figure2.1.5. (c)-(e). Though the resonator pair got interacted, the monopole mode is formed in large region compare with the prior research[6]. It is exactly clear that the peak of new dipole mode founded. It makes more easier optimize THG peak, and this founded feature give a good property to the optical response factors with sharp resonance peak.

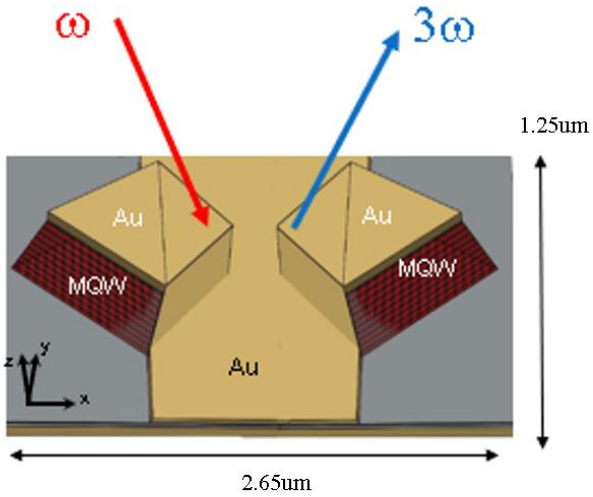

Figure2.1.6. Schematics of meta-atom designs. Unit cell structure of the plasmonic antenna

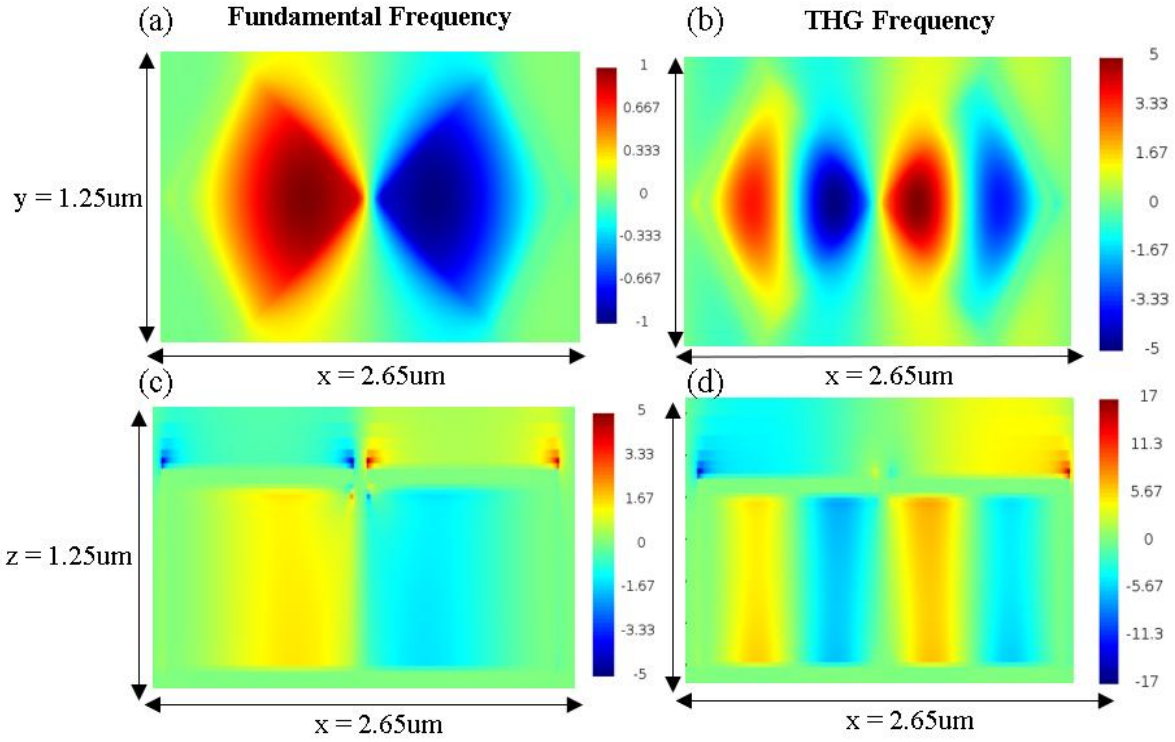

Figure2.1.7 FDTD mode profile results of the top-bottom metal connected kite-shape plasmonic nonlinear metasurfaces. Top-view cross section of the normalized Ez field distribution on the resonator at the (a) Fundamental Frequency (ω) and (b) Third Harmonic frequencies. (3ω) (c)-(d) Side-view the normalized Ez field shown at the (c) FF and (d) TH frequencies.

Synthetically, this kite-shape metasurface can have enhancement of incident E field and then this high enhancement continued to an high E_z field enhancement. Then by connected to top-bottom metal, making monopole interaction which can be interaction region get wider in fundamental frequency, the interaction of incident E field regime, relevant wavelength at 9um. With the combined all this factor, the overlap factor of this structure reaches at 3.15. this make the THG intensity is almost 9 times higher than prior research. And considering the saturation relaxation by the wider interaction region of the incident field.

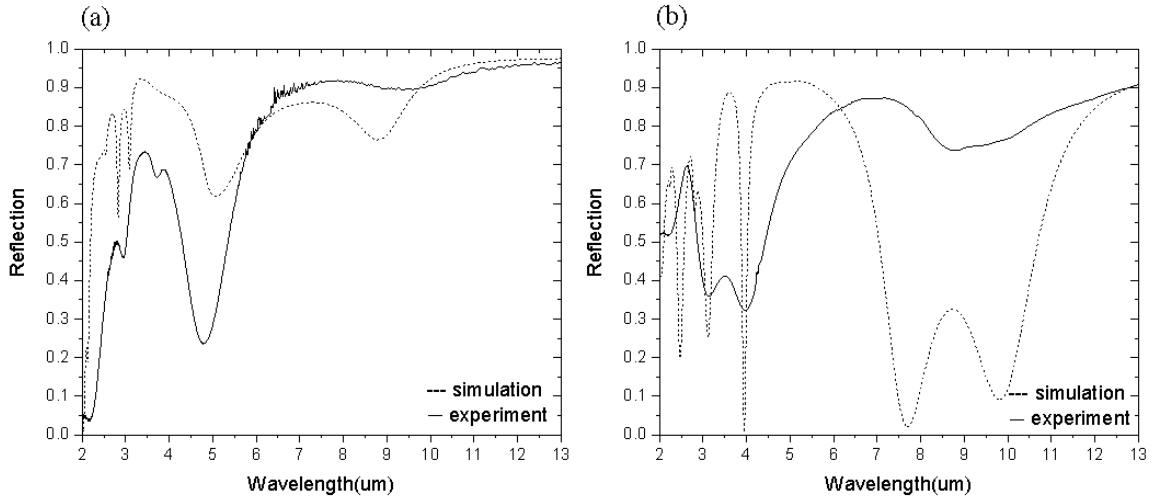

Figure2.1.8. Simulation and experiment results of linear reflection spectra of the nonlinear metasurface for designed metasurface

2.2 Fabrication of the antennas

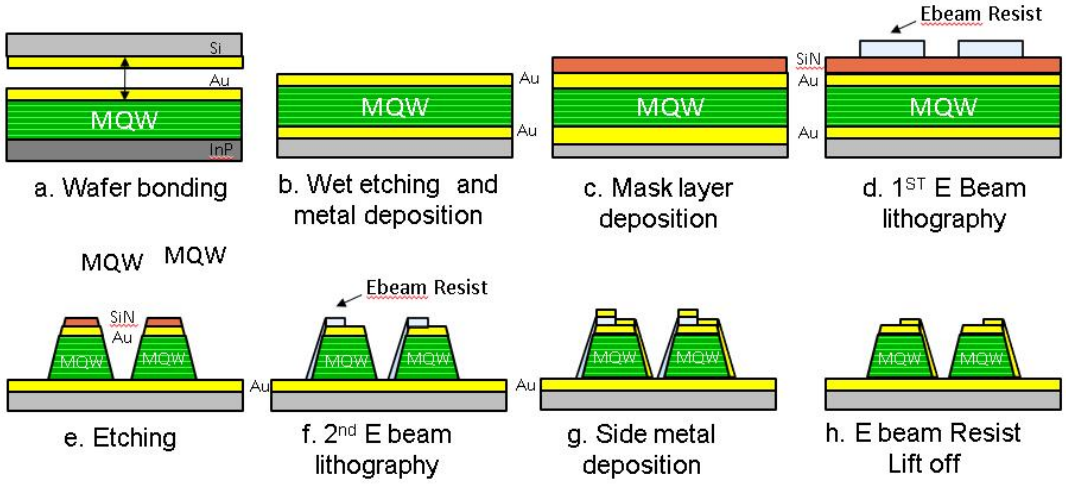

Figure 2.2.1 Schematic of fabrication step of the nonlinear metasurface

2.2.1 Sample Preparation

1. Wafer bonding

The most important thing to notice for sample preparation is to keep the sample clean and safe for contaminations and pollination.

The first step making a nonlinear photonic metasurface is bond a growth MQWs wafer and metal substrate which deposited 10nm of chrome for adhesion layer, 50nm of platinum for blocking the carrier diffusion what make sample defect, 150nm of gold by E beam evaporator on bare Si wafer. for this thermo-compression wafer bonding, generally, between metal and dielectric bonding is hardly strong, so, specially care about the adhesion for metal layer and MQWs layer. In order to improving the adhesion and cleaning MQWs wafer should be oxidated with Reactive Ion Ethching (RIE) (FAB star, O_2 100sccm, for 60sec) and put it in Buffered Oxide Etchant (BOE) for 10seconds. Then put the wafers in pressure chamber with matched align with carbon sheet. The pressure of the chamber is 1kN/cm^2 and heat to 240℃. Chamber reached that temperature, about 6kN of clamping force got applied for 15minutes. When the prosses ended, enough cooling time needed for stable adhesion.

2. Polishing

This step is for remove the MQWs wafer's InP substrate and MQWs wafer's spacer layers(~350um), InGaAs/ InP (300nm/100nm). Firstly, removing target is InP wafer layer. mechanical manual polishing using SiC gel(800grit) until it remains 150um~200um considering the inclined and non-stable thickness

of manual polishing's limitation. Then remove the remains, wet etching processes with HCl: Deionized water(DI water) = 3:1(DI water mix for highly reactive HCl works) until the reaction between solution and InP substrate stopped(etch rate~10um/min). Next step for remove the InGaAs 100nm, wet etching solution H_3PO_4:H_2O_2: DI water = 1:1:38 used. Put sample in the solution until the reaction which color changed of the surface between solution and sample is uniform. Lastly, remove the last spacer layer InP 100nm in HCl: Deionized water= 3:1.

3. Deposition

Because of the former wet etching process, the bottom metal bonded MQWs layer is opened. In the top of the sample, as same as before step, to make adhesion better, MQWs layer is cleaned and oxidated by RIE (FAB star, O_2 100sccm, 40mTorr, RF 100W, for 60sec). In order to make sample for MIM(Metal-Insulator-Metal) structure, top metal layer: 5nm chrome for adhesion layer, 60nm Au for nanoresonator, is deposited by ebeam evaporator. For after etching step, mask layer Si_3N_4 400nm is deposited by plasma-enhanced- chemical vapor (PECVD, PEH-600, deposit temperature 200℃, SiH_4 220sccm, NH_3 50sccm, RF 60W for 495seconds)

2.2.2 First Electron Beam Lithography (EBL) and etching

The prepared sample with above fabrication step, fabricating the nano array structures step is extended. The definite design can be realized by Electron beam lithography. To do this, Electron beam Resist (ER) AR-P-6200.09 is spin coated at 3000rpm twice, (prebake temperature 150℃ 60seconds, baked after double coating temperature 150℃ 120seconds) for 400nm thickness of ER. the nano resonators what I designed are patterned by ELB machine (NB3, current 74Na, voltage 80keV, Dose 1.7C/m^2). After patterning the array, developing the sample at AR600-546 solution for 60seconds.

The next step is etch the rest remaining the designed array part.

First etching is 400nm ER as mask layer, 400nm Si_3N_4 dry etching via inductive coupled plasma(ICP-RIE, FAB star, CF_4 20sccm, CHF_3 30sccm, 4.0mTorr, RF1 150W for plasma acceleration, RF2 1000W for chemical dry etching, for 70seconds). The ER residue are burned via RIE O_2 plasma as same with the sample preparation section, (FAB star, O_2 100sccm, 40mTorr, RF 100W, for 300sec). last etching process is top gold 60nm and MQWs 400nm etching which made MQWs confined to z-field more efficiently, in this situation, remained 400nm Si_3N_4 as mask. Note that for connect top-gold and bottom gold to side metal, all the MQW layers should be etched in this process. The dry etching via inductive coupled plasma (ICP-RIE, FAB star, Cl_2 45sccm, 4.0mTorr, RF1 300W for plasma acceleration, RF2 2000W for physical etching, for 100seconds, selectivity of MQW,gold: $Si_3N_4$2:1).

2.2.3 Second EBL, Side Metal Deposition, and liftoff

Second EBL is for side metal deposition in this process, for align what I designed. The scale in this align width about 1um, it is hardly for photolithography. For this process same machine used(NB3, current 74Na, voltage 80keV, Dose 3.0C/m^2), this time however dose condition highly different because electron beam should get rid of all ER for next fabrication step. ER AR-P-6200.09 is double spin coated at 3000rpm, (prebake temperature 150℃ 60seconds, baked after double coating temperature 150℃ 120seconds) for 400nm thickness of ER.

After the second EBL, chrome 5nm for adhesion layer, Au 60nm for side metal are evaporated via e beam evaporator. Following step for liftoff, put the sample in ER remover approximately 24hours. And using the dropping pipettes, separate the sample with metal residue that fell off with ER. And rinsing with IPA (Isopropanol Alcohol).

(a) (b)

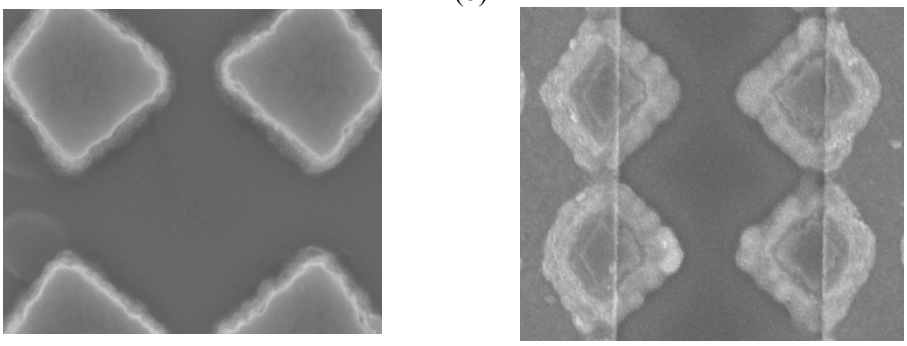

Figure 2.2.2. (a) SEM image of after 1st ebeam lithography and etching (b) SEM image of 2nd ebeam lithography.

2.3 Experiment approach

2.3.1 MQWs Intersubband absorption measurment

(a)

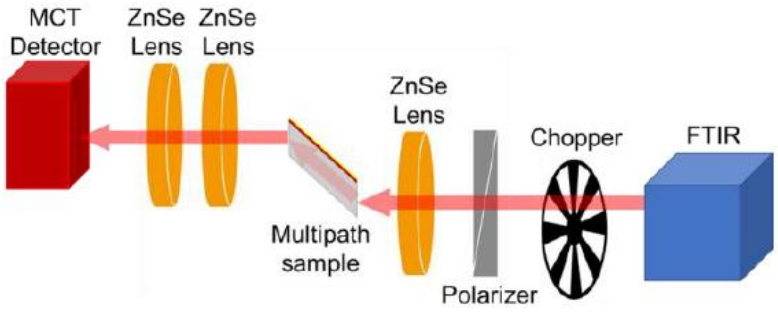

(b)

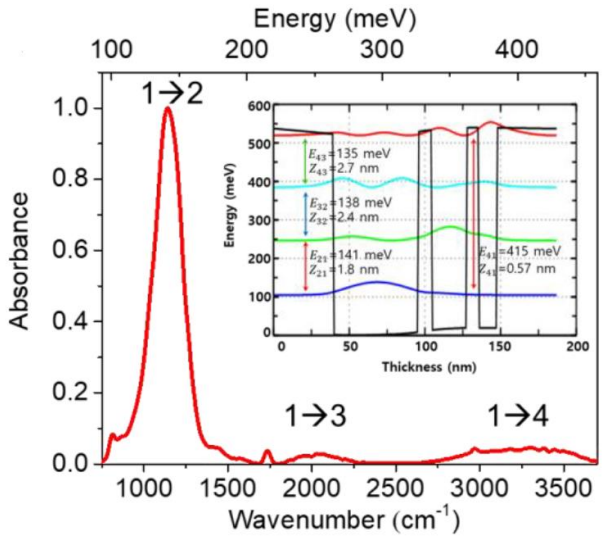

Figure 2.3.1. (a)Intersubband absorption measurement setup. (b) Intersubband absorption spectrum after background correction; the inset shows the conduction band diagram for one period of our MQW structure. [6]

MQWs are a nonlinear medium in this experiment, for extract MQW's intersubband absorption and dielectric constant, separate experiment required. Figure3.3.1 shows measurement setup. MQW sample is polished in backside InP substrate layer as same with the fabrication polishing step,

then deposited back and front side with 100nm thickness of Au. Because of the grown direction, only TM polarized light with an E-field component was absorbed by the intersubband transitions. The TE polarized light intensity is normalized for TM polarized signal. With this optical component the intersubband absorption confficient α_W and it can be expressed with interaction length defined with

$$L_{int} = \frac{n_p L_{MQW}}{\cos(\theta)}$$

$$\alpha_W = -\frac{1}{L_{int}} \ln(10) \log_{10}\left(\frac{I_{TM}}{I_{TE}}\right)$$

In this experiment, θ=45°, L_{MQW}=380nm, n_p=6(estimated value). For MQWs Intersubband absorption measurement, unpolarized mid-IR light pass through the polarizer then converted into TM polarized light from Fourier Transform Infrared Spectrometer (FTIR, Bruker Vertex 70) passes through a chopper and linear polarizer and is focused onto one facet of the multipath sample by a ZnSe lens. Mid-IR light that passes through the multipath sample is then the TM polarized light source passed in MQW sample several times, is then focused onto MCT detector (Infrared Associate, Inc.). [5]

Figure 3.3.1(b) shows the measured intersubband absorption spectrum. The intersubband transition energies were measured to be $E_{21} = \hbar\omega_{21} \approx 141meV$, $E_{31} = \hbar\omega_{31} \approx 252meV$, $E_{41} = \hbar\omega_{41} \approx 407meV$, which matched well with the calculated values shown in Figure 3.3.1.(b) The measured transition linewidths were $2\hbar\gamma_{12} \approx 24meV$, $2\hbar\gamma_{13} \approx 34.6meV$, and $2\hbar\gamma_{14} \approx 44meV$ for the 1–2, 2–3, 1–3, and 1–4 transitions, respectively.[5] The intersubband absorption coefficients for each transition peak were calculated.[7] considering the sample geometry and the thickness of the MQW layer was 400-nm-thick and the number of passes the MQW layer estimated reasonably at 3 times. The calculated intersubband absorption coefficients, respectively α_W were 5.73 × 10^3 cm^{-1}, 2.06 × 10^3 cm^{-1}, 4.02 × 10^2 cm^{-1} and 2.60 × 10^2 cm^{-1} for the 1–2, 2–3, 1–3, and 1–4 transitions. The imaginary part of the out-of-plane dielectric constant of the MQW layer $\varepsilon_\perp$, which related to the absorption α_W, and it can be expressed as

$$\alpha_W = \frac{4\pi}{\lambda} Im(\sqrt{\varepsilon_\perp})$$

(2.3.1)

$$\varepsilon_{\perp}(\omega) \approx \varepsilon_{core}(\omega) + \frac{e^2 N_e}{\varepsilon_0 \hbar}\left[\frac{z_{12}^2}{(\omega_{21}-\omega)-i\gamma_{21}} + \frac{z_{23}^2}{(\omega_{32}-\omega)-i\gamma_{32}} + \frac{z_{13}^2}{(\omega_{31}-\omega)-i\gamma_{31}} + \frac{z_{14}^2}{(\omega_{41}-\omega)-i\gamma_{41}}\right]$$

(2.3.2)

where ω indicates the pump frequency, ε_{core} indicates the averaged dielectric constant of the un-doped semiconductor, N_e is averaged bulk doping density, e is the electron charge, and $\hbar\omega_{ij}$ is energy, $\hbar\gamma_{ij}$ is linewidth and z_{ij} is dipole moment between i and j subband energy level. The dielectric constant of the MQW for the in-plane E-field polarization ($\varepsilon_{\parallel}$) can be expressed as

$$\varepsilon_{\parallel}(\omega) \approx \varepsilon_{core}(\omega) + i\frac{N_e e^2 \tau_D}{\varepsilon_0 \omega m^*(1 - i\omega\tau_D)}$$

(2.4.3)

where $\tau_D \approx 10^{-13}s$ for Drude relaxation time. Using the calculated dielectric constants of the MQW for the out-of-plane ($\varepsilon_{\perp}$) and in-plane ($\varepsilon_{\parallel}$) E-field polarizations, it is applied in to designed MQW layer in the FDTD simulation.

2.3.2 Nonlinear Optical Characterization

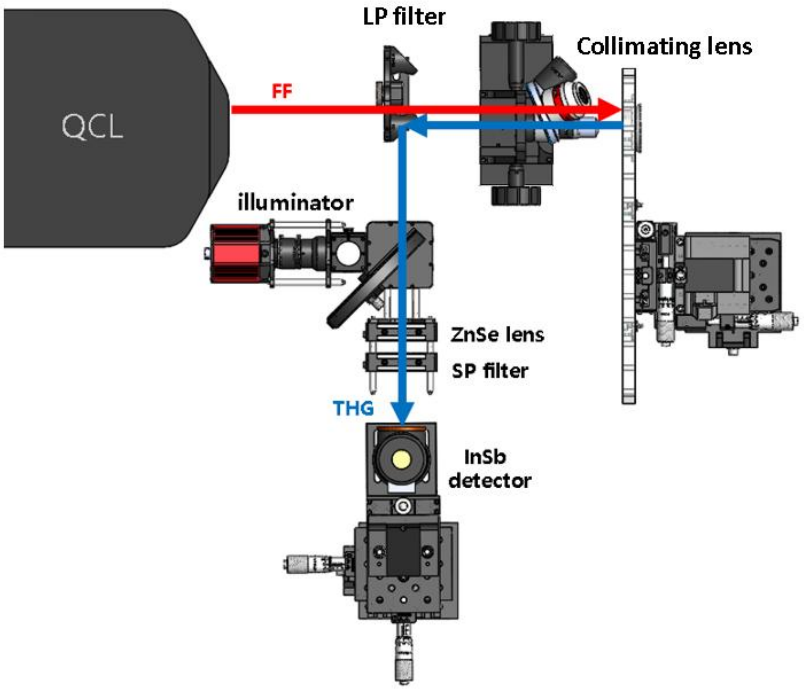

Figure2.3.2 Nonlinear optical measurement setup.

To make a THG optical characterization in fabricated metasurface, Figure3.3.2 shows the optical set up. wavelength-tunable Quantum Cascade Laser (QCL) as laser source in fundamental frequency (FF) lase out with the linearly polarized light. QCL condition as repetition rate:50 kHz, duty cycle 5% and current 1300mA. This beam firstly gets through a long-pass filter as dichroic mirror to reflecting the harmonic generation signal from the QCL and perfectly passes the input pump to the sample, collimating lens to the sample.[6] The THG signal generated from the sample is collected by the same lens and directed to the InSb detector through a polarizer, a ZnSe lens, and a short-pass (SP) filter to blocking the reflected beam with the pump frequency from the sample. The polarization states of the input and output beams are controlled by the sample mounted on a rotational stage and the polarizer. The wavelength of the QCL is 9um (MQW absorption peak) fixed, Input peak intensity and power were measured by power and energy meter (PM100D, Thorlabs) in front of the collimating lens.

(a) (b)

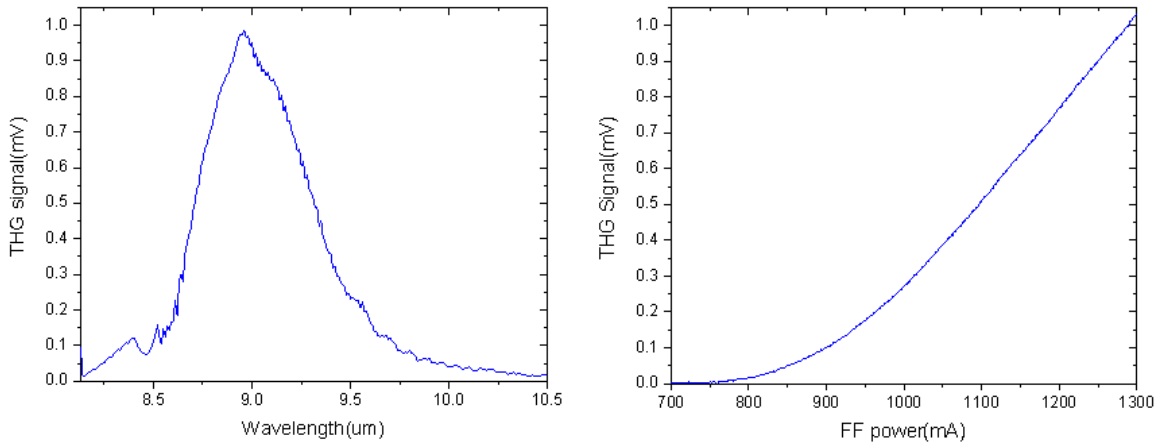

Figure2.3.3. The experimental result of nonlinear characterization. (a)In fundamental frequency,9um, the THG signal in Locking amplifier. (b)The THG signal in variation in laser FF power

2.4 Conclusion

As the result of nonlinear characterization, the result does not match with what I expected. This result can analyze in two ways. This research, the align to connect top-bottom metal what I designed, is decided in 2nd e beam lithography step. And this design assumed the perfect etching of straight top to bottom metal, but the e beam lithography align is not fixed what I want, and the etching result is quite inclined. The result as matched with the designed, more exquisite fabrication step required.

However this deficient fabrication results, it can be demonstrate the resonator pair make dipole mode split with make THG response.

III. Outlook

Using connected top-metal connected plasmonic structure for forming monopole mode, it also can be applied for SHG. This outlook for saturation control metasurface design that depeleted 1st energy level carrier makes nonlinear response get lowered. Just blocking or relax this effect, nonlinear efficiency gets higher value. Usually, this saturation effect considers after measurement step. Not when design the metasurface. This outlook is simulation result of considering saturation effect itself at design metasurface step. The monopole mode forming structure has large area for interaction. This means it is easier to split the mode compared with the other structure.

$$\chi_{ijk}^{eff(2)} = \chi_{zzz}^{(2)} \left\langle \frac{E_{z(i)}^{2\omega}}{E_{i(inc)}^{3\omega}} \cdot \frac{E_{z(j)}^{\omega}}{E_{j(inc)}^{\omega}} \cdot \frac{E_{z(k)}^{\omega}}{E_{k(inc)}^{\omega}} \right\rangle, (i,j,k,=x,y) \tag{3.1}$$

$$S^{SHG} = \frac{1}{2} \frac{I_{S12}^{\omega 1} - I_{z}^{\omega 1}}{I_{S12}^{\omega 1} + I_{z}^{\omega 1}} \tag{3.2}$$

Equation (3.1) is the effective susceptibility of in the polarization of incident electromagnetic field of metasurface. it is defined with the chi of MQW itself and integrated value of the converted Ez field as it called overlap factor,[6] $\chi_{zzz}^{(2)}$ is determined value by grown MQWs. Equation (3.2) is definition of saturation factor in MQW response in SHG.

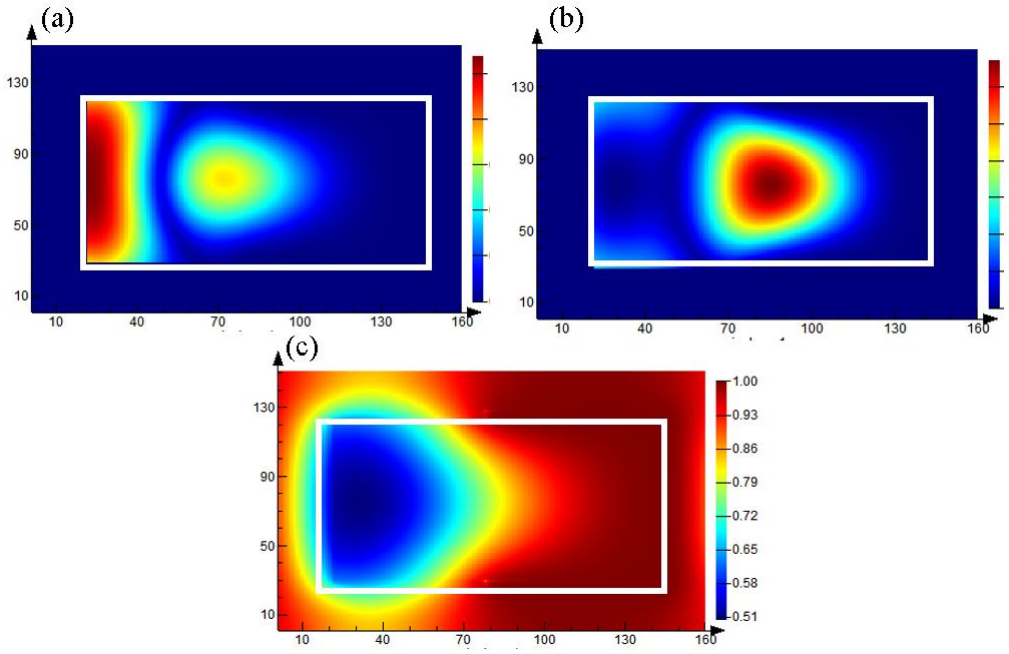

Figure 3.1.(a) mode profile of overlap factor in SHG case of (a) not considering saturation (b) considering the saturation (c)Saturation factor distribution

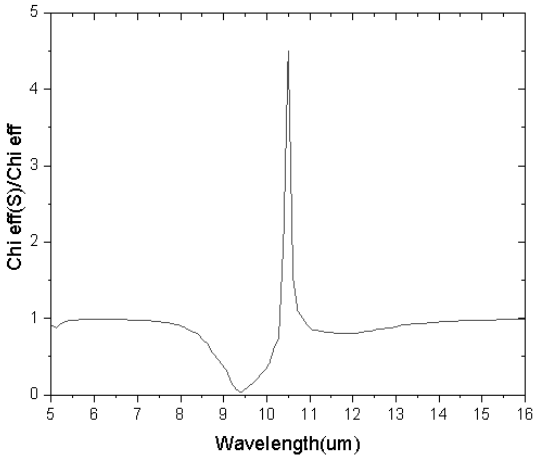

Figure 3.2. the ratio between effective susceptibility of considering saturation and normal susceptibility.

Using this monopole structure, I designed SHG nonlinear metasurfaces with MQW absorption wavelength at 10.5um. With the considering the saturation effect when designed the structure, the effective susceptibility with saturation defined with the multiplying the factors. And saturation always smaller or same than 1, this is the decreased factor of nonlinear efficiency. Tranditionally, the effective susceptibility value is got high value on the same state which saturation is high. It makes effective nonlinearity got decreased, but with the monopole structure, which can make mode spilt quite easier, can differentiate the effective chi modes. With the multiplying the saturation value in mode split effective chi, region in high saturation relaxing and the other mode dominates the effective chi in large region. This makes 4-10 times higher actual effective susceptibility on this structure.

V. Conclusion

I designed nonlinear photonic metasurfaces that can be produced a giant third-order nonlinear response. Combining the structure with MQWs that have giant third-order nonlinearities between four-electron intersubbands transitions with polarization control for a plasmonic nanoresonator. In addition, getting out of the traditional mode, making a monopole-like mode for large E field enhancement region to reduce the saturation that depeleted 1st energy level carrier. Also considering the interaction between the resonators, formed the forbidden newly dipole mode in sharp resonance peak. and experimentally demonstrate the dipole mode split. This result not sufficient with the simulation result, I expect the more elaborate fabrication step can make this result almost same with the simulation result level.

This nonlinear meta surface is highly relaxed phase matching steps and operating power of laser intersity also several tens to hundreds of kilowatts per square centimeter. It can be said that this structure has highly sensitive feature, and it means this structure suited with various applications such as bioimaging, spectroscopy, and sensing.

REFERENCES

1. Almeida, E.; Bitton, O.; Prior, Y., Nonlinear metamaterials for holography. *Nature Communications* **2016,** *7*, 12533.

2. Alexander Krasnok, Mykhailo Tymchenko, Andrea Alù,Nonlinear metasurfaces: a paradigm shift in nonlinear optics,Materials Today,Volume 21, Issue 1,2018,Pages 8-21,

3 Fiore, A., Berger, V., Rosencher, E. *et al.* Phase matching using an isotropic nonlinear optical material. *Nature* **391,** 463–466 (1998)

4. Taher Zahedi, Zaker Hossein Firouzeh, and Abolghasem Zeidaabadi Nezhad, "Design and modeling of third-harmonic plasmonic metasurfaces coupled to multi-quantum well structures," J. Opt. Soc. Am. B 36, 2429-2437 (2019)

5. Towards an optimized all lattice-matched InAlAs/InGaAsP/InGaAs multijunction solar cell with efficiency >50%, Appl. Phys. Lett. 102, 033901 (2013);

6. Yu, J., Park, S., Hwang, I., Kim, D., Jung, J. Y., Lee, J., Advanced Optical Materials 2019, 7, 1801510.

7. Lee, J., Tymchenko, M., Argyropoulos, C. et al. Giant nonlinear response from plasmonic metasurfaces coupled to intersubband transitions. Nature 511, 65–69 (2014).

8. R.W. Boyd, Nonlinear Optics, third ed., Academic Press, 2008.

9. Alexander Krasnok, Mykhailo Tymchenko, Andrea Alù, Nonlinear metasurfaces: a paradigm shift in nonlinear optics, Materials Today, Volume 21, Issue 1, 2018, Pages 8-21, ISSN 1369-7021,

10. Tang, W. X., Zhang, H. C., Ma, H. F., Jiang, W. X., Cui, T. J., Advanced Optical Materials 2019, 7, 1800421.

11. Experimental Verification of a Negative Index of Refraction BY R. A. SHELBY, D. R. SMITH, S. SCHULTZ SCIENCE06 APR 2001 : 77-79 SCIENCE10 NOV 2006 : 977-980

12. Metamaterial Electromagnetic Cloak at Microwave Frequencies BY D. SCHURIG, J. J. MOCK, B. J. JUSTICE, S. A. CUMMER, J. B. PENDRY, A. F. STARR, D. R. SMITH

13. Kim, D., Chung, H., Yu, J., Hwang, I., Park, S., Demmerle, F., Boehm, G., Amann, M. C., Belkin, M. A., Jung, J. Y., Lee, J., Spin Controlled Nonlinear Harmonic Generations from Plasmonic Metasurfaces Coupled to Intersubband Transitions. Adv. Optical Mater. 2020, 8, 2000004.

14. Shape-Controlled Synthesis and Surface Plasmonic Properties of Metallic Nanostructures – Younan Xia et al., MRS Bulletin (2005)

15. Loclalized surface plasmon resonance: Nanostructures, bioassays and biosensing – A review – Eleonora Petryayeva et al., Analytica Chimica Acta 706 (2011)

16. Tang, W. X., Zhang, H. C., Ma, H. F., Jiang, W. X., Cui, T. J., Advanced Optical Materials 2019, 7, 1800421

17. Kasani, S., Curtin, K., & Wu, N. (2019). A review of 2D and 3D plasmonic nanostructure array patterns: fabrication, light management and sensing applications, Nanophotonics, 8(12), 2065-2089

18. Sub-diffraction-limit semiconductor resonators operating on the fundamental magnetic resonance E. Strupiechonski, G. Xu, M. Brekenfeld, Y. Todorov, N. Isac et al. Appl. Phys. Lett. 100, 131113 (2012)

19. Lee, J.; Nookala, N.; Gomez-Diaz, J. S.; Tymchenko, M.; Demmerle, F.; Boehm, G.; Amann, M. C.; Alu, A.; Belkin, M. A., Ultrathin Second-Harmonic Metasurfaces with Record-High Nonlinear Optical Response. *Advanced Optical Materials* **2016,** *4* (5), 664-67

20. Ye, W. M.; Zeuner, F.; Li, X.; Reineke, B.; He, S.; Qiu, C. W.; Liu, J.; Wang, Y. T.; Zhang, S.; Zentgraf, T., Spin and wavelength multiplexed nonlinear metasurface holography. *Nature Communications* **2016,** *7*, 11930.

21. Bhagavantam, S.; Chandrasekhar, P. In *Harmonic generation and selection rules in nonlinear optics*, Proceedings of the Indian Academy of Sciences-Section A, Springer: 1972; pp 13-20.

22. Yu, N. F.; Capasso, F., Flat optics with designer metasurfaces. *Nature Materials* **2014,** *13* (2), 139-150.

23. N. Segal, S. Keren-Zur, N. Hendler, and T. Ellenbogen, "Controlling light with metamaterial-based nonlinear photonic crystals," *Nat.Photonics* 9, 180 (2015).

24 Dasgupta, A., Gao, J., Yang, X., Anisotropic Third Harmonic Generation in Layered Germanium Selenide. Laser & Photonics Reviews 2020, 14, 1900416.

25. Giant Nonlinear Circular Dichroism from Intersubband Polaritonic Metasurfaces
Daeik Kim, Jaeyeon Yu, Inyong Hwang, Seongjin Park, Frederic Demmerle, Gerhard Boehm, Markus-Christian Amann, Mikhail A. Belkin, and Jongwon Lee Nano Lett. 2020, 20, 11, 8032–8039
Publication Date:October 28, 2020

26. Light Propagation with Phase Discontinuities: Generalized Laws of Reflection and Refraction
BY NANFANG YU, PATRICE GENEVET, MIKHAIL A. KATS, FRANCESCO AIETA, JEAN-PHILIPPE TETIENNE, FEDERICO CAPASSO, ZENO GABURRO SCIENCE21 OCT 2011: 333-337